RESEARCH ARTICLE

Editor's Choice

ADVANCED MATERIALS INTERFACES

www.advmatinterfaces.de

Elucidating the Step-Wise Solid Electrolyte Interphase Formation in Lithium-Ion Batteries with Operando Raman Spectroscopy

*Neeha Gogoi, Tim Melin, and Erik J. Berg**

The solid electrolyte interphase (SEI) is arguably one of the most critical components of the Li-ion cell. Despite decades of studies of the SEI, its intrinsic complexity and the lack of suitable characterization tools still prevent a real consensus on the governing mechanisms to be reached. Herein, operando Raman spectroscopy supported by complimentary online electrochemical mass spectrometry is employed to study the SEI formation on Au in a model electrolyte based on $LiClO_4$ in ethylene carbonate (EC). Both the electrolyte itself and cell contaminants, such as O_2, CO_2, and H_2O, contribute in step-wise electro-/chemical processes to the build-up of the SEI. Effects associated with electrode/electrolyte double-layer charging, electrode adsorbate polarization (stark effect), and SEI dissolution are discerned. Lithium carbonate and lithium oxide are identified as major products formed already ≈2 V versus Li^+/Li. Although Raman spectroscopy provides deeper insights into the underlying mechanisms, complementary techniques are necessary to support spectral interpretations. Classical challenges in the field of surface science, such as contaminations, have to be systematically addressed if the puzzle of the SEI ever will be completed.

1. Introduction

Li-ion batteries (LIBs) are found in evermore applications as technical advancements, such as improved cell designs, charging protocols, and battery management systems, alongside new chemistries continue to enhance their performance. Still, several fundamental processes governing these devices are yet to be fully understood. Arguably, one of the most critical aspects is the Solid Electrolyte Interphase (SEI) forming on the negative Li-ion battery electrode during the first few dis-/charge cycles of the cell. Electrolytes in LIBs are generally not cathodically stable and reductively decompose at potentials at which the negative Li-ion graphite electrode operates. Depending on electrolyte composition, the resulting decomposition products may in turn form a protective passivating layer, an SEI, on the surface of the negative electrode. An ideal well-formed SEI is chemically stable, non-dissolving, and prevents further solvent degradation while still allowing for sufficient Li^+-ion transport between the electrolyte and electrode during dis-/charge. The composition, structure, and formation mechanism of the SEI is still debated despite thousands of studies.[1–4] The first model of the SEI was presented in 1979 and further developed in 1983 by Peled[5,6] who postulated that the SEI consists of two layers: a compact thin inner layer and a porous outer layer. In 1995, Aurbach et al. proposed that the inner layer consists of inorganic species, such as LiF and Li_2O, while organic species such as lithium alkyl carbonates are found in the outer layer.[7] A few years later, Peled presented another model where the SEI consists of solvent- and salt-derived organic and inorganic domains mixed in a mosaic structure,[8] which until today is the most accepted model. Nearly all LIB electrolytes contain ethylene carbonate (EC) as a major solvent, which upon decomposition is a prime contributor to the SEI.[2] Although most studies use virtually identical EC-based electrolytes, i.e., 1 M of a Li-salt ($LiPF_6$ or $LiClO_4$) dissolved in a mixture of EC and a linear carbonate (typically dimethyl carbonate (DMC), diethyl carbonate (DEC), or ethyl methyl carbonate (EMC)), there is a very wide spread in the reported SEI compositions ranging from organic alkyl carbonate, semi-carbonates, oxalates, glycols, olefins, to inorganic halides, oxides and hydroxides.[3] This spread can to some extent be explained by the difference in the purity of the electrolytes. Contaminants react both chemically and electrochemically with several cell components forming unwanted products that either are soluble in the electrolyte or precipitate to contribute to the SEI. For instance, water is a well-known contaminant in LIBs and due to the hygroscopicity of the electrolyte, separators and electrodes,[9–11] it is notoriously difficult to avoid, and may have a drastic influence on the performance as well as the composition of the SEI through hydrolysis of electrolyte salt, solvents and SEI species.[3,12]

N. Gogoi, T. Melin, E. J. Berg
Department of Chemistry
Ångström Laboratory
Uppsala University
Box 538, Uppsala SE-751 21, Sweden
E-mail: erik.berg@kemi.uu.se

The ORCID identification number(s) for the author(s) of this article can be found under https://doi.org/10.1002/admi.202200945.

DOI: 10.1002/admi.202200945

Another source of inconsistencies in our understanding of the SEI is the wide spread of methodologies used for its characterization. Considering its nanometric dimensions, the most commonly used analytical technique to study the SEI is X-ray Photoelectron Spectroscopy (XPS), but Vibrational Spectroscopy in form of Fourier Transform Infrared (FTIR) or Raman Spectroscopy has also been extensively used.[13] Typically ex situ analysis is applied, i.e., electrodes are first cycled inside normal battery cells, then extracted, washed, and transferred to the spectrometer for analysis. During these steps, there is a high possibility for the SEI to further react with the solvent used for washing or other contaminants present in the same solvent, or glovebox, or transfer chambers, etc. Additional effects of washing could also be partial dissolution of the SEI and transformation of meta-stable to stable SEI compounds.[13,14] As a consequence, the layer analyzed is not identical to the native SEI on the electrode during cell operation. Accordingly, limited information on the composition and little to no information on the formation or evolution of the SEI is obtained by ex situ measurements. Focus of attention has therefore increasingly been directed toward in situ and operando techniques capable of analyzing the SEI during formation/operation.[15] Already in 1991, Goren et al. presented diverse in situ infrared spectroscopy setups to study SEI formation process.[16] Later, Imhof and Novák used in situ FTIR to study electrochemical reduction of carbonate electrolytes on carbon.[17] In this study, as well as in a later in situ FTIR study by Novák,[18] the spectral response is found to be dominated by changes in Li^+-coordination in the electrolyte as Li is consumed at the electrode surface during its polarization and essentially no signal from eventual SEI species is detected. In situ Raman spectroscopy has in a likewise manner been employed in several configurations[19–22] similarly providing only minor indications of possible SEI species. In fact, the nm-thin SEIs constitute only a minute fraction of the typically micron-sized light-analyte interaction volumes in conventional vibration spectroscopy, which together with the low sensitivity of vibrational spectroscopy (percentages of analyte needed for detection) makes resolving and deconvoluting the vibrations of SEI species from bulk electrolyte vibrations close to impossible. In order to retrieve information primarily from nm-structured SEI by utilizing IR and visual light, the diffraction limit has in principle to be beaten, e.g. by resorting to nonlinear and surface-sensitive vibrational spectroscopic techniques. One prominent example is Vibrational Sum-Frequency Generation (SFG), which is a nonlinear coherent vibrational spectroscopic technique that during the past decade has been employed to study SEI formation.[23–27] Even though SFG spectroscopy is a powerful, well-suited technique for interface studies, it is only found in a few studies likely due to the complexity of experimental execution and data analysis. Two further approaches are Surface-Enhanced Infrared Absorption Spectroscopy (SEIRAS) and Surface-Enhanced Raman Spectroscopy (SERS), which employ similar cell configurations as conventional in situ IR and Raman spectroscopy, but exploit the strong light-analyte interactions at nanostructured coinage metal surfaces. To the best of our knowledge, no in situ SEIRAS study on specifically electrolyte reduction or SEI formation has been published so far, likely because of the poor enhancement factor and the limited choice of suitable Attenuated Total Reflectance (ATR)-crystals. SERS on the other hand has been claimed to be employed for in situ studies of SEI formation[28–33] due to the high intrinsic surface sensitivity, simple set-up, and commercially available optimized SERS substrates. Sang-Don Han et al. employed in situ SERS to study the composition of the SEI on a silicon anode and correlated the spectroscopic observations with the electrochemical performance of the electrode.[32] A recent work from our lab showed that when a model Au SERS substrate is negatively polarized, charging of the electric double layer appears to be directly observed until the formation of SEI, which subsequently dominates the spectral response.[31] The extent to which Raman signal from the SEI components is enhanced by the Au surface appears comparatively low. The operando methodology showed however that electrolyte impurities, such as hydrogen fluoride and water, even present in trace amounts significantly contribute to an SEI dominated by LiF and Li_2CO_3 formed in multistep (electro-)chemical processes. Furthermore, advanced Raman spectroscopy substrates include the shell-isolated nanoparticle-enhanced Raman spectroscopy (SHINERS), first employed by Hy et al. to investigate the SEI formation on Si and Cu electrodes.[29] It was followed by the work by Galloway et al.[34] and Cabo-Fernandez et al.[35] where they probe the surface layer formed upon Li metal and C-coated $Zn_{0.9}Fe_{0.1}O$ electrodes respectively. Even more recently, Gajan et al. employed the SHINERS approach under operando conditions to track the dynamic evolution of the SEI on Au and Sn electrodes upon cycling of LIB cells.[33] Classical experimental challenges commonly found in the field of surface science, such as influence of impurities, were however not addressed. Several details of experimental conditions, such as electrode composition/morphology, electrolyte volume (flooding factor) and purity, etc. often lead to misleading results and markedly influence data reproducibility. Model systems may therefore be resorted to in order to reduce complexity, such as introduced by the multicomposite electrode and electrolyte structures found in Li-ion batteries. Decreasing the number of components, e.g. by introducing a more well-defined single-element surface and simple electrolyte should reduce the likelihood of unexpected reactions and the spread in possible products, thus facilitating spectral deconvolution and analysis. The conceivably most simple electrolyte would contain only a single solvent and single salt. EC is the archetype Li-ion battery solvent and has a well-known SEI forming capability on the negative electrode. $LiClO_4$ is known for its chemical stability relative to the more commonly used $LiPF_6$, which is easily hydrolyzed to highly reactive PF_5 and HF. Herein, a model electrolyte based on $LiClO_4$ in EC mixed in 1:6 molar ratio (hereafter denoted "$LiClO_4$:EC") is investigated.

The aim of the current study is to determine the step-wise SEI formation process on an Au SERS substrate immersed in an EC-based single-solvent electrolyte during the first reductive sweep. Complementarily to Raman analysis, Online Electrochemical Mass Spectrometry (OEMS) is utilized to characterize volatile gaseous products from the SEI formation. In addition, we will illustrate and discuss methodological possibilities and technical limitations with our operando Raman spectroscopy.

2. Results and Discussion

2.1. Current Profile and Associated Gas Evolution

Figure 1a shows the current response from the Au working electrode in the OEMS cell as well as in the Raman cell during the first cathodic potential sweep (0.1 mV s^{-1}) from 2.5 V versus Li^+/Li (hereafter all potentials are relative to the Li^+/Li redox potential) to 0.5 V in $LiClO_4$:EC (1:6 molar ratio). Deviation between the two current profiles can be explained by the varying OEMS and Raman cell geometries, which result in different ratios between electrolyte volume to electrode area, cell resistance and mass transport limitations. Mainly three common features in the current response are discerned (marked by dashed lines at 2.0, 1.6, and 1.0 V in Figure 1b), all of which can be assigned to unique gas evolution processes. The first process starting at 2.0 V is assigned to EC reduction, which typically is associated with two well-established reaction pathways: a single-electron (per EC molecule) reduction pathway (reaction 1) often reported to result in lithium ethylene dicarbonate ($(CH_2COCO_2Li)_2$, LEDC) and a two-electron reduction pathway (reaction 2) resulting in Li_2CO_3:

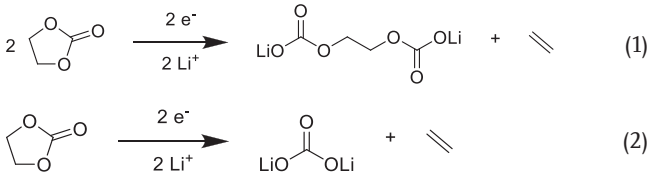

(1)

(2)

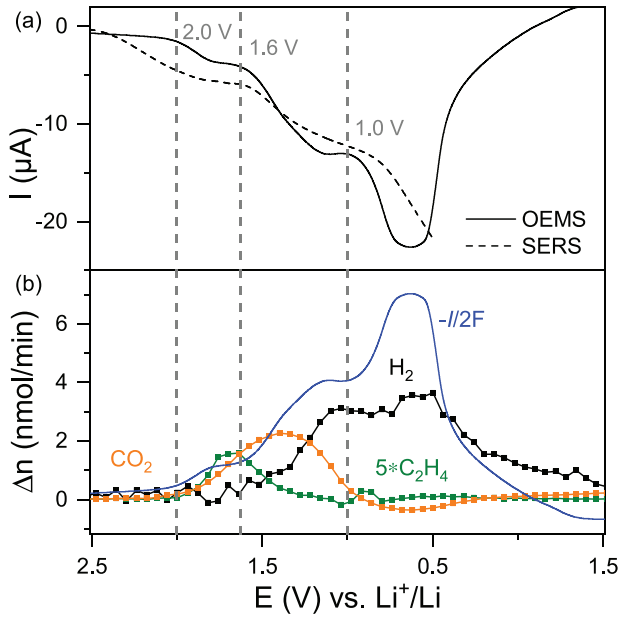

Figure 1. a) Current response, *I*, of an Au working electrode in the OEMS cell (solid line) and an Au SERS substrate in the operando Raman cell (dashed line, scaled with a factor of 18 to fit the same current axis). b) Gas evolution rate, Δn, of the main gases (orange CO_2, green C_2H_4, and black H_2) evolved. All data presented is from the first cathodic potential sweep (0.1 mV s^{-1}) in $LiClO_4$:EC (1:6 molar ratio).

Since both reactions lead to C_2H_4, distinguishing between the two is not possible with OEMS. Reduction of EC is generally assumed to occur <1.0 V,[2] although most studies are performed on C-electrodes, and the electrocatalytic properties of Au are expected to shift the reduction potential to higher electrode potentials. Indeed, C_2H_4 evolution on Au was already observed at ≈2.0 V in a typical battery electrolyte by us, but not further discussed at the time.[31]

CO_2 evolution starts roughly at the same potential as C_2H_4 and increases monotonically until 1.4 V. Studies in our team have shown that the CO_2 evolution starts however already at higher potentials of ≈2.6 V and is independent of C_2H_4 evolution. Organic carbonate-based electrolytes can dissolve a significant amount of CO_2, which makes it difficult to determine the exact on-set potential of this process. Since no reduction current is associated with this process, CO_2 derives from a chemical reaction likely initiated by the electrochemical reduction of oxygen (E_{ORR} ≈3.0 V) possibly adsorbed on the Au surface (reaction 3):

$$Au - O_n + e^- \rightarrow Au - O_n^- \quad (3)$$

Previous studies of Li-air batteries with organic carbonate based electrolytes have shown that oxygen reduction leads to oxides that in turn chemically ring-open EC through a nucleophilic attack on the ethereal carbon.[36–38] The ring-opened EC is highly reactive and subsequently undergoes multiple chemical reaction steps leading to alkoxycarbonate radicals. These radicals can in turn initiate an autocatalytic ring-opening reaction of EC forming polyethylene glycol (PEG^-) and CO_2 according to:

(4)

hence explaining the observed continuous evolution of CO_2. Starting at ≈1.6 V, the second electrochemical process is dominated by H_2 evolution (in black in Figure 1b, compare with blue line, representing the current converted into gas evolution rate assuming two moles electrons per mol gas) likely originating from trace H_2O reduction (reaction 5):

$$H_2O + e^- \rightarrow OH^- + \frac{1}{2}H_2 \quad (5)$$

As discussed in the introduction, water is notoriously difficult to avoid and ppm-level H_2O residues always remain despite thorough drying procedures of all cell components. The resulting hydroxides are known to chemically react with cyclic carbonates similar to the radical described in reaction 4, even though OH^- is more prone to attack the carbonyl-carbon. Again, the ring-opened EC is expected to continue to react autocatalytically with EC forming PEG (according to reaction 4). No correlation between CO_2 and H_2 evolution is however found, which could be explained by the higher concentration of Li^+ in the electrolyte, which likely lowers the propensity of OH^- to react by forming LiOH. CO_2 evolution decreases at <1.4 V and even a net negative gas evolution rate (i.e., CO_2 consumption) occurs at <1 V. Two processes consuming CO_2 are foreseen, one C-E reaction (chemical step followed by an electrochemical step, namely reaction 6 combined with reaction 7) and one pure electrochemical reduction of CO_2 (reaction 8). OH^- and CO_2 are

in equilibrium with bicarbonate (reaction 6) that can be electrochemically reduced to Li_2CO_3 (reaction 7).

$$OH^- + O_2 \rightleftharpoons HCO_3^- \quad (6)$$

$$HCO_3^- + e^- + Li^+ \rightarrow Li_2CO_3 + \frac{1}{2}H_2 \quad (7)$$

$$2Li^+ + 2CO_2 + 2e^- \rightarrow Li_2C_2O_4 \quad (8)$$

The third electrochemical process sets in at <1.0 V accompanied by a further slight increase in H_2 evolution rate accelerated by the lower electrode potentials. Possibly, the reduction of bicarbonate (reaction 7) sets in here, which in turn shifts the equilibrium in reaction 6 and CO_2/OH^- is consumed hence contributing to the consumption of CO_2 in this region. Direct reduction of CO_2 is also expected, possibly forming Li-oxalate that does not result in any gas evolution (reaction 8), which could explain the deviation between the current and observed gas evolution before the cut-off at 0.5 V is reached.

2.2. Operando Raman Spectroscopy

Figure 2a shows extended Raman spectra (200 to 3250 cm^{-1}) of $LiClO_4$:EC on an Au SERS substrate at OCP and 0.5 V. The main spectral features at OCP stem from the electrolyte, namely the vibrational bands of free and Li^+-coordinated EC as well as one symmetric stretch mode of ClO_4^- (marked by vertical dashed lines, c.f. table of assignments in SI). Additional peaks in the OCP spectrum at 292, 521, and 2133 cm^{-1} are attributed to the Au-O_n like species, first optical phonon of Si (dashed green line) and Au−O=C like species (dashed red line), respectively. Adsorbed O_n and O=C like species, such as O_2 and CO_2, are expected on the Au substrate because of its prior air exposure before entering the Ar-filled glovebox. The Si phonon mode originates from the SERS substrate (Si nanopillars coated with Au).[39] In Figure 2b, three wavenumber-regions of the operando Raman spectra (from OCP to 0.5 V) are presented as contour plots. There are changes in intensities for the electrolyte induced Raman bands, the appearance of new signals as well as shifts in peak position of Au-bonded species. In order to elucidate the potential dependence of the vibration bands in the Raman measurement, specific spectral regions as well as fitted intensities of main peaks are highlighted in **Figure 3**a,b, respectively.

Spectral features associated with the electrolyte itself (namely EC, Li^+ solvated by EC denoted EC-Li^+, and ClO_4^-) are predominantly found in the regions 700–800, 850–950, and 1350–1700 cm^{-1}. Initially, the EC-Li^+ bands (727 and 905 cm^{-1}) show significant increase in intensity with a maximum at 2.3 V. At potentials <2 V, a synchronous drop in peak intensity for all vibration bands is observed and correlates with the onset in electrochemical reduction current (Figure 1a). Increase in EC-Li^+ peak intensity upon negative electrode polarisation was previously reported by us,[31] though for a slightly different electrolyte composition, and assigned to the build-up of coordinated EC during charging of the electric double layer (EDL) at the Au electrode. However, contrary to the previous observation, a minor increase is also observed in the intensity of the vibrational mode corresponding to free/uncoordinated EC at 717 and

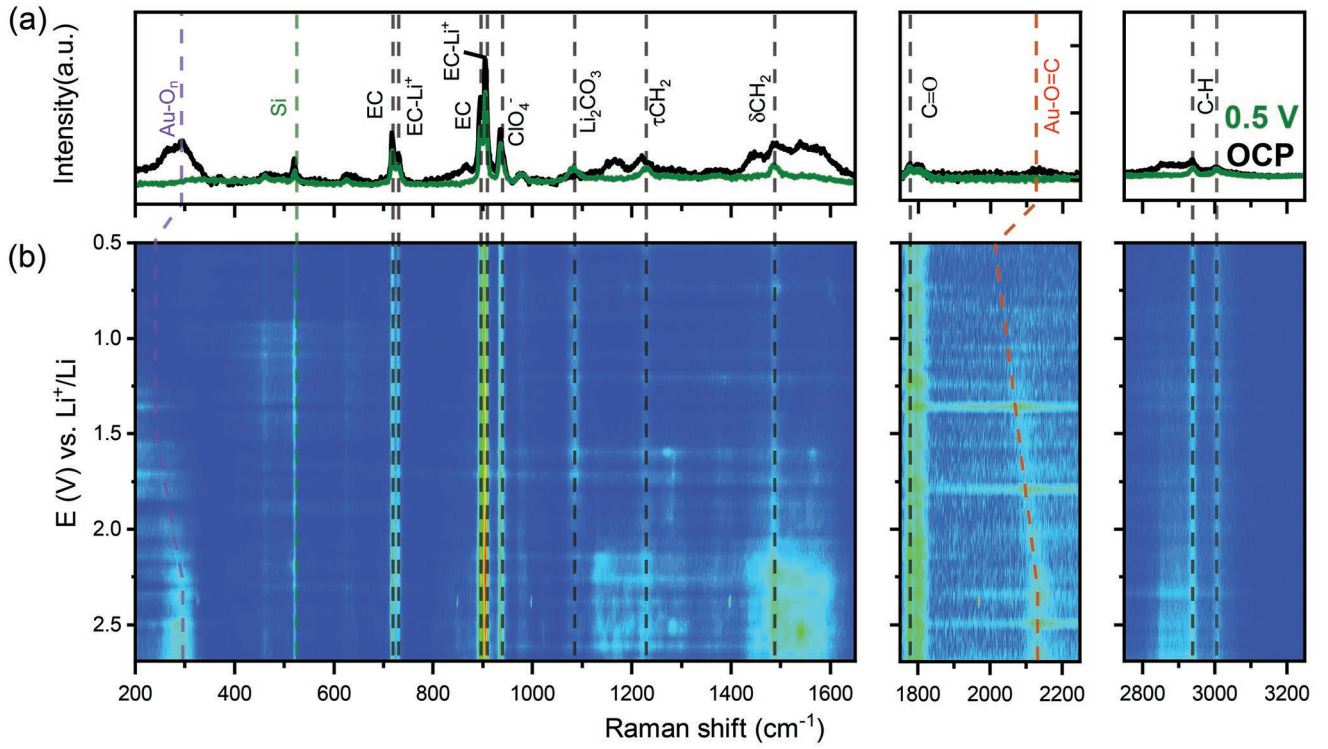

Figure 2. a) Raman spectra at OCP (black) and 0.5 V (green) and b) Contour plot showing operando Raman spectra during the first reduction half cycle of an Au SERS substrate used as working electrode in $LiClO_4$:EC.

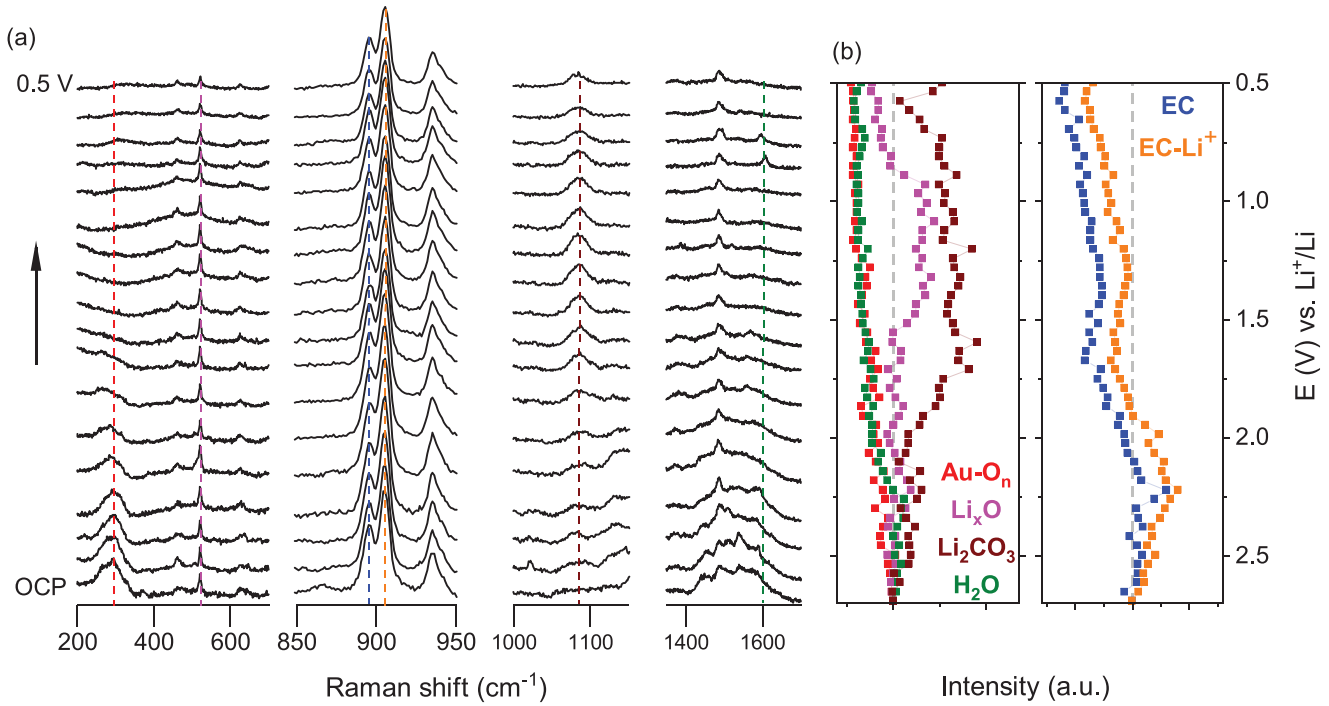

Figure 3. a) Characteristic spectral features responding to the applied potential from OCP (bottom) until 0.5 V (top), b) fitted intensities of the selected Raman peaks. Each fitted intensity is normalized against the intensity of the peak in the OCP spectrum.

894 cm^{-1}. Clearly, the solvent–salt coordination structure is different in the higher salt concentrated electrolyte studied herein and it is not clear to what extent the peaks at 717 and 894 cm^{-1} actually belong to uncoordinated EC. The symmetric stretch mode of ClO_4^- at 934 cm^{-1} remains virtually constant, except for a minor decline starting at ≈2 V. The perchlorate anion likely stays in the electrolyte bulk throughout the whole experiment and the associated peak follows the general trend of reduced intensity as the Au surface turns less reflective because of the build-up of the SEI.

A broad Raman band at 292 cm^{-1} could be associated with the Au—O_n type species,[40] which in line with reaction 3 is gradually electrochemically reduced. Another broad peak is observed at around 1140 cm^{-1} down to ≈2 V. This peak lies in the region of superoxide stretch (assigned to the O—O stretch mode of superoxide, $\nu(O_2^-)$,[41] which further strengthens our claim. Negatively charged surface oxygen could initiate EC ring opening according to reaction 4 and hence explain the early evolution of CO_2 (Figure 1b). Meanwhile, a band at 523 cm^{-1} associated with Li_xO grows, although the overlap with the Si phonon band at 521 cm^{-1} renders a clear deconvolution of these two bands difficult.[42] In any case, lithium oxides are reactive toward both EC and CO_2, which would lead to the formation of more thermodynamically stable products, such as Li_2CO_3, on the Au surface.

Indeed, in Figure 2b an emerging band at 1085 cm^{-1} is observed at <2 V, which is a characteristic vibration band of Li_2CO_3 that together with the concomitant C_2H_4 evolution in the OEMS measurement (Figure 1b) would support the proposed two-electron reduction pathway of EC (reaction 2). The intensity of the band remains constant until 1.0 V where a small decrease is observed, but the band is still present until 0.5 V meaning Li_2CO_3 stays on the electrode surface. No spectral evidence of LEDC can be identified.

Another observation is the fading of peaks around 1600 cm^{-1}, which are likely associated with surface contaminants. For instance, H_2O generally appears as a broad peak at 1617 cm^{-1} and these peaks are found to fade away at the same time as when H_2 is observed to evolve. Additionally, two very minor peaks appearing at OCP at ≈460 cm^{-1} and 620 cm^{-1} increase in intensity during negative polarization. However, the assignments of these two signals are unclear and could be related to some intermediate species.

As mentioned above, the signal at 2133 cm^{-1} observed at the OCP Raman spectrum is identified as O=CR adsorbed on the uncoordinated Au sites. CO_2 is a known electrolyte impurity, generally formed upon electrolyte degradation. The intensity of the band slowly decreases and shifts to 2070 cm^{-1}, and is visible down to a potential of ≈1.1 V. This shift as a function of applied potential is due to the Stark effect, and is indicative of chemisorbed species on the electrode surface. This Stark tuning effect with a rate of ≈36 cm^{-1} V^{-1} is however, more than what has been reported earlier.[43] A similar behavior is also observed for the signal at 292 cm^{-1}. It appears at OCV and slowly shifts to 272 cm^{-1} at ≈1.9 V and is thus again suggestive of Au metal-adsorbate interactions.

However, all of the peaks associated with the electrolyte and the SEI decrease in intensity as the electrode is polarized to even lower potentials (Figure 3b). Interestingly, also the Rayleigh peak as well as the autofluorescence background are observed to decrease in intensity upon negative polarization. The formation of a layer on the Au surface likely reduces light reflection, which results in less photon scattering into the spectrometer. The SEI layer is therefore in part Raman inactive and

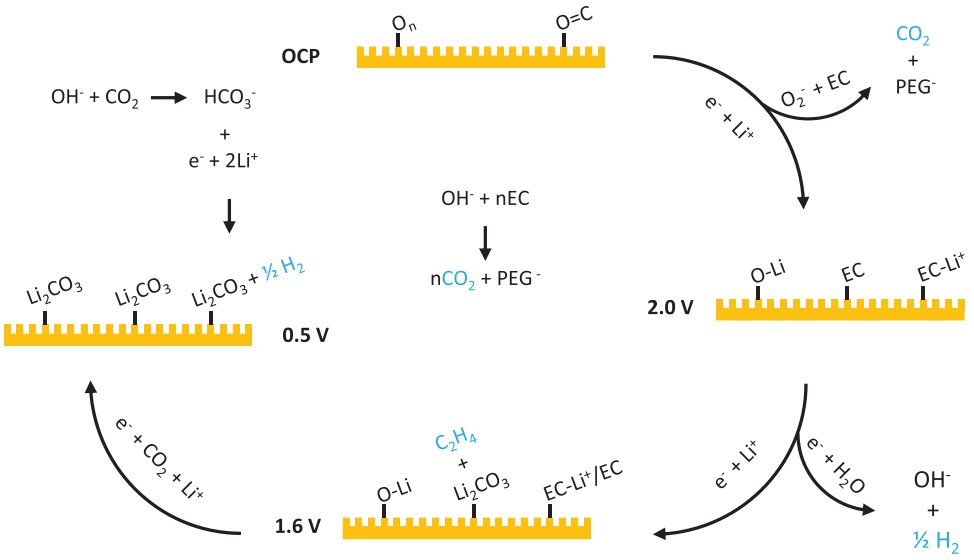

Figure 4. Schematic summary of the most prominent reaction taking place during SEI formation. Light blue species are volatile and detectible with OEMS.

hence not detected. This conclusion is strengthened by looking into the intensity profile after the cell has been stopped, while Raman spectra were still recorded. Upon fitting, it was found that the intensities of the peaks again rise, indicating that the layer thus formed dissolves into the electrolyte and allows light to reflect back into the spectrometer. Working with a commercially validated SERS Au substrate as electrode, the question arises to what extent is the Raman scattering actually surface-enhanced. Early in this study, Raman measurements on Au SERS substrate and planar Au-foil in contact with a Li-ion battery electrolyte were compared and little to no difference in peak intensity between the two substrates was found (see Figure S1 in Supporting Information). The organic carbonate electrolyte therefore appears to have a moderate interaction with the Au surface, although spectral features of Au-molecular interactions are observed, as discussed above. Even if the surface-enhancement of the Au SERS substrate is very minor or next to nothing, the Au surface is highly reflective (more photons are scattered into the spectrometer) and its nano-structured roughness provides a higher electrode area (lower flooding factor) compared to planar Au.[44]

Finally, multiple replicates of identical cells with the same electrolyte were performed and a spread in results between cells is observed (Figure S2, Supporting Information). The most common difference between the cells is often observed at >2.0 V in the region 1200–1600 cm^{-1} associated with electrolyte contaminants, which is also a conceivable result from the human factor. However, most essential features such as the change in the ratio between free and coordinated EC and appearance of Li_2CO_3 are constantly reproduced in all cells.

3. Conclusion

In summary, we investigated the real-time formation of solid electrolyte interphase (SEI) using operando Raman spectroscopy. For that, an Au SERS substrate is negatively polarized from 3.0 V down to 0.5 V versus Li^+/Li in a 1:6 $LiClO_4$:EC model electrolyte. Our study provides further details on the SEI formation mechanisms, which are found to be triggered by multiple electro-/chemical processes. Most importantly, the influential role of impurities in the battery cell is evidenced. Observations are summarized in **Figure 4**. First, surface-contaminating Au-adsorbates were found to reduce and form Li_xO type species as the first depositing SEI component. Then, direct observation of charging of the electric double layer was made. Another crucial finding is the electrochemical reduction of EC at around 2 V, earlier than reported before when compared to typically used carbon-based anode, thus unveiling the catalytic effect of Au. This reduction process takes place by a two-electron pathway leading to Li_2CO_3 as the dominating SEI component, along with the evolution of C_2H_4. The evolution and consumption of CO_2 plays an important role in the interphase formation with both chemically and electrochemically active reduction pathways. The spectroscopic analysis also reveals that, depending on their proximity toward the nanostructured Au surface, SERS activity favors some SEI species over others. As a result, certain species are more enhanced, hence more spectroscopically active, than others. The surface-enhancement of the electrolyte and SEI species from our Au substrates needs further investigation since the current enhancement appears to be relatively low compared to most other SERS substrates encountered in the literature. Impurities belong to one of the most classical experimental challenges in surface science and typically also strongly affect SEI electrochemistry, especially in model studies with small surface area electrodes in contact with a surplus of electrolyte. Environmental gases, such as O_2, H_2O, and CO_2, remain and even form to different degrees in/on cell components, after which they eventually diffuse, adsorb and partake in electrode surface electrochemistry. Even minor differences in electrode/electrolyte preparation processes (e.g., washing, drying, etc.) lead to varying concentrations of cell contaminants and result in irreproducible and frequently misleading data. Established practices from the field of surface science are

therefore advised including excessive drying and exact control of electrolyte composition. Alternatively, predefined concentrations of contaminants can be added to systematically investigate their influence on the electrode/electrolyte system under study. Regardless of the methodology, a meticulous approach with careful control of impurities is necessary to successfully reveal the formation and evolution mechanism of the SEI.

4. Experimental Section

1:6 (molar ratio) $LiClO_4$:EC electrolyte mixture was prepared and stored in Ar-filled glove box. $LiClO_4$ and EC were used as received from Sigma-Aldrich. 25 ppm H_2O was determined by Karl Fischer Titration. The Au SERS substrates (Au on nanostructured Si (3 mm×3 mm)) were purchased from Silmeco company.[39] The operando measurements were performed in a custom-made spectroelectrochemical cell where SERS Au is used as the working electrode and a lithium foil as the counter electrode filled with 50 µL of $LiClO_4$:EC electrolyte. The Li foil was pierced in the middle of 1 mm diameter hole. The laser beam impinges the Au substrate through the hole in the Li and the electrolyte.

The Raman spectra were obtained from Renishaw Raman spectrometer InVia, 2013, with a laser power source of wavelength of 785 nm (laser power 1.5 mW) and grating of 1200 lines mm^{-1}. The acquisition time for one Raman spectrum was 100 s (20 s × 5 accumulations). The standard mode laser spot size is ≈1.5 µm at 50× magnification. Raman spectroscopy was performed during the same time as reducing the electrolyte on the Au. Autofluorescence background was corrected with the WIRE 3.4 software package (Renishaw Inc.) and the fitting was performed manually by using a Python-script for least-square minimization of a Lorentzian type peak.

The battery cell design is described in Mozhzhukhina et al.[31] with minor adaptations made. Linear sweep voltammetry was performed from OCP down to 0.5 V versus Li^+/Li with a scan rate of 0.025 mV s^{-1}.

The Au working electrodes for the OEMS measurements were prepared by coating stainless-steel mesh (212/90 µm, Bopp AG, Switzerland) with ≈50 nm Au on each side by sputter deposition at room temperature. In each cell, two circular Au-coated mesh electrodes (∅ 15 mm) were used as working electrodes. To avoid gas evolution from the counter electrode, $LiFePO_4$ electrodes (∅ 15 mm, Custom cells, 2 mAh cm^{-2}, Germany) were punched and delitihiated to 3.43 V versus Li^+/Li before assembly. The OEMS cell and the data treatment procedure has been described in previous publication.[45] Linear sweep voltammetry was performed from OCP down to 0.5 V versus Li^+/Li with a scan rate of 0.1 mV s^{-1}.

Supporting Information

Supporting Information is available from the Wiley Online Library or from the author.

Acknowledgements

N.G. and T.M. contributed equally to the work. The authors acknowledge Knut and Alice Wallenberg (KAW) Foundation (Grant 2017.0204), Swedish Research Council (2016-04069), Stiftelsen för Strategisk Forskning (SSF, FFL18-0269) for financial support and StandUp for Energy for base funding.

Conflict of Interest

The authors declare no conflict of interest.

Data Availability Statement

The data that support the findings of this study are available from the corresponding author upon reasonable request.

Keywords

interphases, Li-ion batteries, operando, Raman, solid electrolyte interphase, SERS

Received: April 28, 2022
Revised: June 9, 2022
Published online: July 8, 2022

[1] M. Winter, *Z. Phys. Chem.* **2009**, *223*, 1395.
[2] K. Xu, *Chem. Rev.* **2014**, *114*, 11503.
[3] S. J. An, J. Li, C. Daniel, D. Mohanty, S. Nagpure, D. L. Wood, *Carbon* **2016**, *105*, 52.
[4] E. Peled, S. Menkin, *J. Electrochem. Soc.* **2017**, *164*, A1703.
[5] E. Peled, *J. Electrochem. Soc.* **1979**, *126*, 2047.
[6] E. Peled, *J. Power Sources* **1983**, *9*, 253.
[7] A. Zaban, D. Aurbach, *J. Power Sources* **1995**, *54*, 289.
[8] E. Peled, D. Golodnitsky, G. Ardel, *J. Electrochem. Soc.* **1997**, *144*, L208.
[9] M. Stich, N. Pandey, A. Bund, *J. Power Sources* **2017**, *364*, 84.
[10] J. C. Eser, B. Deichmann, T. Wirsching, P. G. Weidler, P. Scharfer, W. Schabel, *Langmuir* **2020**, *36*, 6193.
[11] F. Huttner, W. Haselrieder, A. Kwade, *Energy Technol.* **2020**, *8*, 1900245.
[12] P. G. Kitz, P. Novák, E. J. Berg, *ACS Appl. Mater. Interfaces* **2020**, *12*, 15934.
[13] P. Verma, P. Maire, P. Novák, *Electrochim. Acta* **2010**, *55*, 6332.
[14] L. Somerville, J. Bareño, P. Jennings, A. McGordon, C. Lyness, I. Bloom, *Electrochim. Acta* **2016**, *206*, 70.
[15] L. Meyer, N. Saqib, J. Porter, *J. Electrochem. Soc.* **2021**, *168*, 090561.
[16] E. Goren, O. Chusid (Youngman), D. Aurbach, *J. Electrochem. Soc.* **1991**, *138*, L6.
[17] R. Imhof, P. Novák, *J. Electrochem. Soc.* **1998**, *145*, 1081.
[18] S. Pérez-Villar, P. Lanz, H. Schneider, P. Novák, *Electrochim. Acta* **2013**, *106*, 506.
[19] M. Inaba, H. Yoshida, Z. Ogumi, T. Abe, Y. Mizutani, M. Asano, *J. Electrochem. Soc.* **1995**, *142*, 20.
[20] J.-C. Panitz, F. Joho, P. Novák, *Appl. Spectrosc.* **1999**, *53*, 1188.
[21] P. Novák, D. Goers, L. J. Hardwick, M. Holzapfel, W. Scheifele, J. Ufheil, A. Würsig, *J. Power Sources* **2005**, *146*, 15.
[22] L. J. Hardwick, H. Buqa, M. Holzapfel, W. Scheifele, F. Krumeich, P. Novák, *Electrochim. Acta* **2007**, *52*, 4884.
[23] P. Mukherjee, A. Lagutchev, D. D. Dlott, *J. Electrochem. Soc.* **2012**, *159*, A244.
[24] B. G. Nicolau, N. García-Rey, B. Dryzhakov, D. D. Dlott, *J. Phys. Chem. C* **2015**, *119*, 10227.
[25] Y. Horowitz, H.-L. Han, P. N. Ross, G. A. Somorjai, *J. Am. Chem. Soc.* **2016**, *138*, 726.
[26] Y. Horowitz, H. L. Han, G. A. Somorjai, *Ind. Eng. Chem. Res.* **2018**, *57*, 1480.
[27] A. Ge, D. Zhou, K. I. Inoue, Y. Chen, S. Ye, *J. Phys. Chem. C* **2020**, *124*, 17538.
[28] R. Schmitz, R. Ansgar Müller, R. Wilhelm Schmitz, C. Schreiner, M. Kunze, A. Lex-Balducci, S. Passerini, M. Winter, *J. Power Sources* **2013**, *233*, 110.
[29] S. Hy, Felix, Y. H. Chen, J. Y. Liu, J. Rick, B. J. Hwang, *J. Power Sources* **2014**, *256*, 324.

[30] G. Yang, I. N. Ivanov, R. E. Ruther, R. L. Sacci, V. Subjakova, D. T. Hallinan, J. Nanda, *ACS Nano* **2018**, *12*, 10159.
[31] N. Mozhzhukhina, E. Flores, R. Lundström, V. Nyström, P. G. Kitz, K. Edström, E. J. Berg, *J. Phys. Chem. Lett.* **2020**, *11*, 4119.
[32] Y. Ha, B. J. T. de Villers, Z. Li, Y. Xu, P. Stradins, A. Zakutayev, A. Burrell, S.-D. Han, *J. Phys. Chem. Lett.* **2020**, *11*, 286.
[33] A. Gajan, C. Lecourt, B. E. T. Bautista, L. Fillaud, J. Demeaux, I. T. Lucas, *ACS Energy Lett.* **2021**, *6*, 1757.
[34] T. A. Galloway, L. Cabo-Fernandez, I. M. Aldous, F. Braga, L. J. Hardwick, *Faraday Discuss.* **2017**, *205*, 469.
[35] L. Cabo-Fernandez, D. Bresser, F. Braga, S. Passerini, L. J. Hardwick, *Batteries Supercaps* **2019**, *2*, 168.
[36] S. A. Freunberger, Y. Chen, Z. Peng, J. M. Griffin, L. J. Hardwick, F. Bardé, P. Novák, P. G. Bruce, *J. Am. Chem. Soc.* **2011**, *133*, 8040.
[37] V. S. Bryantsev, M. Blanco, *J. Phys. Chem. Lett.* **2011**, *2*, 379.
[38] J. P. Vivek, N. G. Berry, G. Papageorgiou, R. J. Nichols, L. J. Hardwick, *J. Am. Chem. Soc.* **2016**, *138*, 3745.
[39] M. S. Schmidt, J. Hübner, A. Boisen, *Adv. Mater.* **2012**, *24*, OP11.
[40] J. Kim, A. A. Gewirth, *J. Phys. Chem. B* **2006**, *110*, 2565.
[41] T. A. Galloway, L. J. Hardwick, *J. Phys. Chem. Lett.* **2016**, *7*, 2119.
[42] T. Osaka, I. Shindo, *Solid State Commun.* **1984**, *51*, 421.
[43] M. Moradzaman, G. Mul, *ChemElectroChem* **2021**, *8*, 1478.
[44] T. Melin, R. Lundström, E. J. Berg, *Adv. Mater. Interfaces* **2021**, *9*, 2101258.
[45] R. Lundström, E. J. Berg, *J. Power Sources* **2021**, *485*, 229347.